Clinical Science (2021) **135** 2393–2408
https://doi.org/10.1042/CS20210821

PORTLAND PRESS

Research Article

Chronic activation of AMP-activated protein kinase leads to early-onset polycystic kidney phenotype

Laura Wilson[1], Alice E. Pollard[1,2], Lucy Penfold[1], Phillip J. Muckett[1], Chad Whilding[1], Mohammad Bohlooly-Y.[3], Patricia Wilson[4] and David Carling[1,5]

[1]MRC London Institute of Medical Sciences, Hammersmith Hospital Campus, Imperial College London, W12 0NN U.K.; [2]Structure Biophysics and Fragments, Discovery Sciences, Biopharmaceuticals R&D, AstraZeneca, Cambridge, U.K.; [3]Translational Genomics, Discovery Sciences, BioPharmaceuticals R&D, AstraZeneca, Gothenburg, Sweden; [4]Centre for Nephrology, UCL Department of Renal Medicine, Royal Free Campus, London NW3 2PF, U.K.; [5]Institute of Clinical Sciences, Imperial College London, Hammersmith Hospital, London W12 0NN, U.K.

Correspondence: David Carling (david.carling@lms.mrc.ac.uk)

AMP-activated protein kinase (AMPK) plays a key role in the cellular response to low energy stress and has emerged as an attractive therapeutic target for tackling metabolic diseases. Whilst significant progress has been made regarding the physiological role of AMPK, its function in the kidney remains only partially understood. We use a mouse model expressing a constitutively active mutant of AMPK to investigate the effect of AMPK activation on kidney function *in vivo*. Kidney morphology and changes in gene and protein expression were monitored and serum and urine markers were measured to assess kidney function *in vivo*. Global AMPK activation resulted in an early-onset polycystic kidney phenotype, featuring collecting duct cysts and compromised renal function in adult mice. Mechanistically, the cystic kidneys had increased cAMP levels and ERK activation, increased hexokinase I (Hk I) expression, glycogen accumulation and altered expression of proteins associated with autophagy. Kidney tubule-specific activation of AMPK also resulted in a polycystic phenotype, demonstrating that renal tubular AMPK activation caused the cystogenesis. Importantly, human autosomal dominant polycystic kidney disease (ADPKD) kidney sections revealed similar protein localisation patterns to that observed in the murine cystic kidneys. Our findings show that early-onset chronic AMPK activation leads to a polycystic kidney phenotype, suggesting dysregulated AMPK signalling is a contributing factor in cystogenesis.

Introduction

AMP-activated protein kinase (AMPK) is a highly conserved heterotrimeric enzyme that plays a central role in regulating metabolism. AMPK is composed of three subunits (α, β and γ), each with multiple isoforms [1]. The biological relevance of the existence of these multiple isoforms is currently unclear, however there are substantial differences between isoforms in terms of tissue distribution [1,2]. In response to a decrease in ATP, AMPK is activated leading to an increase in the phosphorylation of its downstream substrates, with the net effect of restoring normal ATP levels within the cell. AMPK promotes ATP-generating processes such as glycolysis, by increasing the expression of glucose transporters and hexokinase [3]. Conversely, AMPK generally inhibits ATP-utilising processes, for example AMPK inhibits mammalian target of rapamycin (mTOR) signalling by phosphorylating the tuberous sclerosis complex 2 (TSC2) and raptor to inhibit protein synthesis and cell growth [4,5]. However, an exception to this generalisation is that chronic AMPK activation results in increased glycogen synthesis in muscle tissue, due to indirect activation of glycogen synthase occurring as a result of enhanced muscle glucose uptake [6].

In the kidney, AMPK has been reported to inhibit the activity of the cystic fibrosis transmembrane conductance regulator (CFTR) chloride channel [7–9] and the epithelial sodium channel, ENaC [10–12]. Because CFTR is thought to play an important role in the fluid secretion that promotes cyst enlargement in

Received: 19 August 2021
Revised: 27 September 2021
Accepted: 07 October 2021

Accepted Manuscript online: 08 October 2021
Version of Record published: 22 October 2021

Clinical Science (2021) **135** 2393–2408
https://doi.org/10.1042/CS20210821

polycystic kidney disease (PKD), AMPK activation has been suggested to be a novel therapeutic strategy for PKD treatment [13]. Pharmacological activation of AMPK has also been shown to have beneficial effects in a tubulointerstitial fibrosis model [14] and to improve kidney function in diabetic nephropathy models [15,16]. More recently, treatment with an AMPK activator has been shown to reduce renal disease severity in a model of TSC1 deletion [17].

In contrast with these short-term studies, the effect of chronic AMPK activation on renal function is largely unknown. One study revealed that mice harbouring an activating mutation in AMPKγ2 exhibit increased renal inflammation, cyst formation and impaired kidney function when fed a high-fat diet [18] suggesting long-term AMPK activation could have detrimental effects. However, the effects of chronic activation of AMPKγ1 on renal function have not currently been explored. To investigate this, we utilised a genetic mouse model where AMPKγ1 is constitutively activated. Here we show that chronic activation of AMPKγ1 resulted in a striking polycystic kidney phenotype, featuring compromised renal function, glycogen accumulation and altered expression of proteins involved in autophagy.

Materials and methods

Mice

All experiments involved in the generation of transgenic animals were approved by Gothenburg Ethics Committee. All *in vivo* studies were performed in accordance with the U.K. Animals Scientific Procedures Act (1986) and approved by the Animal Welfare and Ethical Review Board at Imperial College London. Gain-of-function and wildtype mice were generated as described previously [19]. For widespread expression, mice were crossed with mice harbouring Cre-recombinase under the control of a β-actin promoter (Tmem163Tg(ACTB-cre)2Mrt), on a mixed bl6/129sv background. A kidney tubule-specific model of AMPK activation was generated by crossing with mice harbouring Cre-recombinase under control of the Cdh16 promoter (sometimes referred to as kidney-specific (Ksp)-Cre) [20,21]. Mice were maintained on a 12-h light/dark cycle at 22°C with free access to food (chow-standard breeding diet number 3 obtained from Special Diets Services) and water, group-housed in specific-pathogen free barrier facilities. Mice referred to as 16 weeks old were between 15 and 17 weeks of age at the time of analysis. Unless stated otherwise, male mice were used. Mice were terminally anaesthetised with either isoflurane or carbon dioxide followed by cervical dislocation.

Human kidney sections

Five-micometre-thick paraffin-embedded sections, 4% paraformaldehyde-fixed, age-matched (36–44 years) autosomal dominant polycystic kidney disease (ADPKD) and normal control human kidneys were provided by the PKD Charity-sponsored Bioresource Bank housed at the Royal Free Centre for Nephrology. All nephrectomy samples were collected at source according to Institutional Review Board/NIH approved protocols in U.S.A. and with Royal Free NHS Foundation Trust ethics approval 20772.

Renal phenotyping

Urine kidney injury molecule 1 (Kim-1) and neutrophil gelatinase-associated lipocalin (Ngal) concentrations were determined by ELISA (mouse Kim-1 ELISA kit, Abcam, ab213477, mouse Ngal ELISA kit, R&D Systems, MLCN20). Urine albumin concentration was measured by ELISA with antibodies and standards purchased from Bethyl Laboratories. Creatinine was measured using a Siemens Dimension EXL Auto-analyser. Plasma blood urea nitrogen (BUN) was determined using a commercial BUN assay kit (Invitrogen, EIABUN). Estimated glomerular filtration rate (eGFR) was determined by multiplying the urine creatine concentration by the volume of urine produced per unit time and dividing this value by the serum creatinine concentration. In some cases there was insufficient material to carry out all the analyses on all the mice, so in these cases data shown are for all samples available for analysis.

Histological analysis

Paraformaldehyde (4%)-fixed sections were stained with Haematoxylin and Eosin (H&E). For Periodic Acid–Schiff (PAS) staining, tissues were stained with Periodic Acid and Schiff's reagent followed by counterstaining with Haematoxylin. Stained slides were imaged using an AxioScan slide scanner with 20× magnification objective lens and images were processed using ZEN blue software. For immunofluorescence, slides were imaged using an Olympus IX70 fluorescence microscope with 20× magnification objective lens. Images were then processed using Fiji software. The following antibodies were used for immunohistochemistry and immunofluorescence: anti-AMPKβ1 (Abcam, ab32112), anti-Aquaporin-1 (Abcam, ab15080), anti-Aquaporin-2 (Abcam, ab85876), anti-cleaved caspase 3 (Cell

Signaling Technology, #9661), anti-Hexokinase I (Cell Signaling Technology, #2024), anti-Hexokinase II (Cell Signaling Technology, #2867), anti-NCC (Millipore, AB3553), anti-NKCC2 (LS Biosciences, LS-C313275), anti-TFEB (Bethyl Laboratories, A303-673A). All histological analyses described in the present study were performed blinded with respect to the genotypes and were assessed by two independent researchers.

Cystic index

Cystic index quantification was performed using QuPath (version 0.2.3). Briefly, total tissue area was automatically detected by thresholding, followed by additional thresholding to detect individual cyst candidate regions masked by the total tissue area. Regions detected with an area less than 1500 μm^2 were excluded. Identified regions were visually verified to confirm correct cyst classification, or otherwise removed. Total cystic area was calculated and divided by the total tissue area for calculation of the cystic index.

Measurement of blood pressure

Mice were anaesthetised using isoflurane (4% initially, reduced to 2% during recording) and blood pressure was measured by left carotid telemetry using a fibre-optical pressure sensor (Fiso Technology, QC, Canada, Model FISO-LS-PT9-10) connected to a signal conditioner (Fiso Technology, Model FPI-LS-10). Blood pressure recordings were acquired using Evolution software (Fiso Technology) and analysed using LabChart software to determine systolic blood pressure and diastolic blood pressure. Mean arterial blood pressure was calculated as 1/3 systolic blood pressure plus 2/3 diastolic blood pressure. At the end of the procedure, mice were killed by cervical dislocation.

RNA expression analysis

RNA was extracted from kidneys homogenates using an RNeasy mini kit (Qiagen) and used to synthesise cDNA for analysis. Expression was normalised to *Polr2a* expression and values shown as fold-change. Oligonucleotide primers used in the study: Avpr2 (forward: CCTGGCCATGACACTAGACC, reverse: CATCAAGGCGATCCAGGTGA, expected product size 247 bp), Pkd1 (forward: TCTGGATGGGCTTCAGCAA, reverse: AGCGGGAAGGCAGTGGAT, expected product size 78 bp), Pkd2 (forward: AGACTTCTCGGTGTATAACGCAAA, reverse: CACCCGTTGCTGGGAACT, expected product size 77 bp), Pkhd1 (forward: GAAAGTTAGCCGCCTTGCTG, reverse: AGCTGCTGAGCAAGAGATCC, expected product size 99 bp), Polr2a (forward: CTTCTCTCCCAGTGCTGCAT, reverse: GGGGATGTATGGGCTTGAGG, expected product size 115 bp); mt-CyB (forward: ATTCCTTCATGTCGGACGAG, reverse: ACTGAGAAGCCCCCTCAAAT, expected product size 228 bp) and H19 (forward: GTACCCACCTGTCGTCC, reverse: GTCCACGAGACCAATGACTG, expected product size 207 bp).

Western blotting

Following incubation with primary and secondary antibodies, blots were visualised using the Odyssey Imaging System (LI-COR Biotechnology). Ratio of intensity of the protein of interest was normalised relative to expression of a housekeeping protein. Antibodies used for Western blotting (all at 1:1000 dilution): rabbit anti-P-ACC S79 (Cell Signaling Technology, #3661), rabbit anti-ACC (Cell Signaling Technology, #3676), mouse anti-Akt (Cell Signaling Technology, #2920), rabbit anti-P-Akt S473 (Cell Signaling Technology #3787), rabbit anti-Aldolase A (Cell Signaling Technology, #8060), rabbit anti-AMPKα (Cell Signaling Technology, #2532), mouse anti-ERK1/2 (Cell Signaling Technology, #4696), rabbit anti-P-ERK1/2 T202/Y204 (Cell Signaling Technology, #9101), rabbit anti-Glycogen synthase (Cell Signaling Technology, #3893), rabbit anti-Hexokinase I (Cell Signaling Technology, #2024), rabbit anti-Hexokinase II (Cell Signaling Technology, #2867), rabbit anti-LC3 (Abcam, ab51520), rabbit anti-mTOR (Cell Signaling Technology, #2983), rabbit anti-P70 S6 kinase (Cell Signaling Technology, #2708), rabbit anti-Pgc1α (Abcam, ab54481), rabbit anti-Phosphofructokinase (Cell Signaling Technology, #8164), rabbit anti-Pyruvate dehydrogenase (Cell Signaling Technology, #3205), rabbit anti-PKM2 (Cell Signaling Technology, #4053), mouse anti-S6 (Cell Signaling Technology, #2317), rabbit anti-P-S6 S235/236 (Cell Signaling Technology, #4858), rabbit anti-P-S6 S240/244 (Cell Signaling Technology, #5364), rabbit anti-V-ATPase A (Thermo Scientific, PA5-29191), mouse anti-vinculin (Sigma, V9131-100).

cAMP measurement

Kidneys were analysed for cAMP content using a commercial cAMP assay kit (Abcam, ab65355). The concentration of cAMP in each sample was calculated from a standard curve generated from known cAMP concentrations and normalised to wet tissue weight to determine the concentration of cAMP per milligram of tissue.

Clinical Science (2021) **135** 2393–2408
https://doi.org/10.1042/CS20210821

Mitochondrial content analysis

Mitochondrial content was determined by quantifying the relative amount of mitochondrial to nuclear DNA. DNA was extracted from frozen kidneys using a DNeasy Blood and Tissue DNA Extraction kit (Qiagen). Fifty nanograms of DNA was used per reaction to quantify the expression level of the mitochondrial gene *mt-CyB* (encoding cytochrome *b*) and nuclear gene *H19*.

Glycogen assay

Glycogen content was quantified using a glucose oxidase kit (Sigma–Aldrich, GAGO20-1KT) and plotted relative to wet tissue weight.

Statistical analysis

All data are presented as mean (± SEM). Differences were analysed by two-tailed Student's *t* test or two-way ANOVA, followed by a Bonferroni's multiple comparisons test to determine statistical significance between groups based on one variable. All statistics were performed using GraphPad Prism 8 software.

Results

AMPK activation leads to a polycystic kidney phenotype

We previously reported on a genetic mouse model expressing a gain-of-function mutation in the AMPKγ1 subunit [19,22]. A global model of AMPK activation (hereafter referred to as D316A-Tg) was generated by crossing mice harbouring the floxed D316Aγ1 allele with β-actin-Cre mice. This results in widespread tissue expression of the transgenic AMPKγ1 protein [22]. As a control, mice expressing the wildtype γ1 transgene (WT-Tg) were used. An increase in phosphorylation of acetyl-CoA carboxylase (ACC), a downstream substrate of AMPK, confirmed AMPK activation in the kidney (Supplementary Figure S1). Increased expression of total ACC protein was also evident in kidney lysates from mice expressing the D316A mutant, suggesting compensation in response to ACC inactivation. Consistent with our previous studies, there was no change in the overall expression of total AMPK, as judged by expression of the α1 and α2 subunit isoforms. Upon dissection, it was evident that kidneys from the D316A-Tg mice were larger than kidneys for WT-Tg mice and had numerous macroscopic cysts that were not present in WT-Tg mice (Figure 1A). This polycystic kidney phenotype was dramatic in D316A-Tg mice aged 3 weeks and was still present in mice aged approximately 16 weeks, although with a significantly reduced cystic index (Figure 1B). Kidney weight relative to total bodyweight was significantly higher in D316A-Tg mice compared with WT-Tg mice from 11 days of age onwards (Figure 1C), and consistent with the reduction in cystic index, 16-week-old mice had lower relative kidney weights compared with 3-week-old mice. Both male and female mice showed a similar kidney phenotype (Figure 1D). Daily urine production was increased in the D316A-Tg mice, together with markers of kidney function (Figure 1E). Kim-1, Ngal, plasma creatinine and BUN were all significantly increased in D316A-Tg mice compared with WT-Tg (Figure 1E). The eGFR was modestly reduced in the D316A-Tg mice although this did not reach statistical significance (Supplementary Figure S1). Together, these data indicate that D316A-Tg mice show signs of kidney damage and impaired renal function, but no change in GFR. It should be noted that GFR was estimated using creatinine clearance, an approach that is known to have limitations in rodent models of kidney disease, and so care should be taken when interpreting these results. To further explore the impact of the kidney damage we measured blood pressure in the mice. As shown in Supplementary Figure S1, mean arterial blood pressure is significantly increased in the D316A-Tg mice at 16 weeks of age.

Our initial studies indicated that kidney cysts appear in neonatal mice, so we examined kidneys from mice at 8, 11 and 14 days *postpartum*. H&E-stained kidney sections from D316A-Tg and WT-Tg mice aged 8 days did not reveal any significant changes, and cysts were not observed (Figure 1F). At 11 days *postpartum*, tubular dilations are apparent in the cortical region of the kidney and by 14 days of age tubular dilations and cysts were present in cortical and medullary regions of D316A-Tg kidneys. No glomerular cysts were observed in any of the sections examined. To characterise the origin of the cysts, sections were stained with markers for collecting ducts, proximal tubules, thick ascending limbs of the Loop of Henle and distal convoluted tubules (Figure 1G). Cysts were predominantly formed in the collecting ducts of D316A-Tg kidneys. We did not detect cysts in any other tissues examined, including liver, pancreas and spleen (data not shown).

Altered signaling pathways in kidneys following AMPK activation

To investigate possible mechanisms of how chronic AMPK activation causes renal cystogenesis, expression of genes implicated in PKD pathogenesis was assessed by RT-qPCR. In humans, autosomal dominant (AD) PKD is most

Clinical Science (2021) **135** 2393–2408
https://doi.org/10.1042/CS20210821

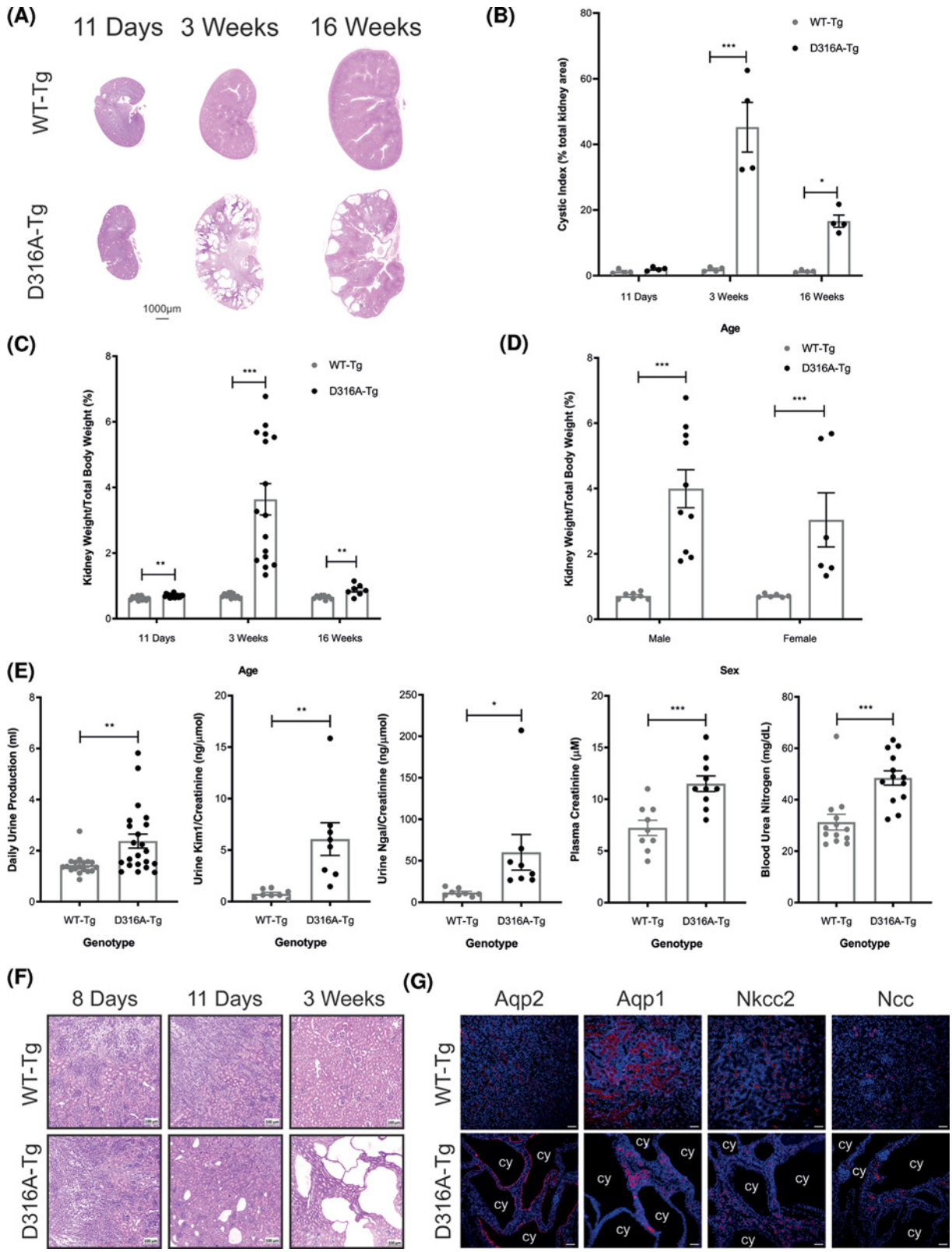

Figure 1. Chronic activation of AMPK leads to a polycystic kidney phenotype

(**A**) H&E staining of kidneys isolated from WT-Tg and D316A-Tg mice at 11 days, 3 and 16 weeks of age. A representative image of each genotype at each time-point is shown. (**B**) Cystic index of kidneys and (**C**) kidney weights expressed as a percentage of total bodyweight harvested from β-actin WT-Tg and β-actin D316A-Tg mice at different ages ($n \geq 4$ mice per genotype and age, male and female mice). (**D**) Kidney to body weight in mice aged 3 weeks separated according to sex is shown (same data as shown in

Clinical Science (2021) **135** 2393–2408
https://doi.org/10.1042/CS20210821

panel C). Data are presented as mean ± SEM and statistical significance determined by Student's *t* test for each age (*$P<0.05$, **$P<0.01$, ***$P<0.001$). (**E**) Daily volume of urine production ($n=18$ for WT-Tg and $n=22$ for D316A-Tg), urine Kim1 and Ngal levels plotted relative to creatinine concentration ($n=8$ per genotype), together with plasma creatinine concentration ($n=9$ for WT-Tg and $n=10$ for D316A-Tg) and BUN concentration ($n=13$). In all cases, data are presented as mean ± SEM and statistically significant differences between genotypes were determined by Student's *t* test (*$P<0.05$, **$P<0.01$, ***$P<0.001$). (**F**) H&E staining of kidney sections taken from WT-Tg and D316A-Tg mice at 8, 11 days and 2 weeks of age. Representative images of four mice per genotype are shown. (**G**) Immunofluorescence staining of kidney sections from mice at 3 weeks of age. Sections were stained with antibodies against either aquaporin 2 (Aqp2), aquaporin 1 (Aqp1), Na-K-Cl cotransporter (NKCC2) and thiazide-sensitive Na-Cl cotransporter (NCC) (shown in red) and nuclei counterstained with DAPI (blue). Cysts are indicated with 'cy' and scale bar represents 50 μm. A representative image for each genotype at each age is shown. Similar data were obtained using sections isolated from kidneys from at least three other mice.

commonly associated with mutations in *PKD1* or *PKD2* [23–25] and autosomal recessive (AR) PKD is caused by mutations in *PKHD1* [26,27]. Expression of *Pkd1*, *Pkd2* and *Pkhd1* was not changed in kidneys from D316A-Tg mice relative to WT-Tg (Supplementary Figure S2). We next investigated the possible involvement of dysregulated cAMP-Erk and Akt-mTOR signalling, as these pathways have previously been shown to be involved in PKD pathogenesis [28–32] and AMPK is known to negatively regulate mTOR signalling [4,5]. There was an increase in the ratio of phosphorylated Erk1/2 (T202/Y204) to total Erk1/2, together with a modest increase in the ratio of phospho-Akt (S473) to total Akt in D316A-Tg kidneys at 11 days of age (Figure 2A,B), a stage when tubule dilations are evident. Moreover, increased cAMP levels were detected in D316A-Tg kidneys at 11 days of age, and by 3 weeks of age (in highly cystic kidneys) this difference was dramatically amplified (Figure 2C). Increased expression of the vasopressin receptor (V2R), encoded by *Avpr2*, has been reported in PKD models and hyperactivation of V2R is believed to be responsible for elevated renal cAMP levels in PKD [30,33–36]. A significant decrease in *Avpr2* expression was observed in kidneys taken from D316A-Tg mice at 11 days old. However, by 3 weeks of age, *Avpr2* expression was significantly up-regulated in D316A-Tg relative to WT-Tg kidneys (Figure 2D). Although mTOR and p70 S6 kinase protein expression were elevated in D316A-Tg kidneys aged 11 days, no differences in phosphorylated S6 (a downstream target of mTOR) were observed compared with WT-Tg kidneys (Supplementary Figure S3), suggesting that increased mTOR activity may not be a contributing mechanism to the PKD phenotype.

Metabolic changes in the kidney in response to AMPK activation

We previously reported a significant increase in mitochondrial biogenesis in white adipose tissue in the D316A-Tg model [22]. At 11 days of age there was no change in expression of peroxisome proliferator activated receptor-γ co-activator 1α (Pgc1α), a transcription factor known to regulate mitochondrial biogenesis [37] in kidney lysates from D316A-Tg mice compared with WT-Tg (Supplementary Figure S4). Consistent with Pgc1α expression, no differences in kidney mitochondrial content were observed between genotypes at 11 days, however at 3 weeks of age mitochondrial content in D316A-Tg kidneys was significantly reduced compared with WT-Tg (Supplementary Figure S4). Recently, metabolic reprogramming has emerged as an important feature in renal cystogenesis [38] with reduced mitochondrial metabolism and increased aerobic glycolysis being reported in cystic kidneys [39–41]. As AMPK is known to play an important role in regulating glucose metabolism, we studied the expression of glycolytic enzymes in this model. Expression of hexokinase I (Hk I), but not hexokinase II (Hk II), was significantly up-regulated in D316A-Tg compared with WT-Tg kidneys at 11 days of age (Figure 3A–C). Hk I was expressed in the cyst-lining cells of D316A-Tg kidneys and localised to the distal tubules and collecting ducts, whereas Hk II was primarily expressed in the proximal tubules, and was not detected in cells lining the cysts in D316A-Tg kidneys (Figure 3C). No significant changes in expression of other glycolytic enzymes were detected, apart from a modest increase in pyruvate dehydrogenase in D316A-Tg kidneys compared with WT-Tg (Supplementary Figure S5).

A consequence of chronic AMPK activation is increased glycogen accumulation in heart and skeletal muscle [2] and interestingly there was a significant increase in glycogen levels in kidneys from 14-day-old D316A-Tg mice compared with WT-Tg mice (Figure 3D). Furthermore, PAS staining for glycogen revealed accumulation in cells near the dilating tubules of kidneys from 11-day-old D316A-Tg mice, which was not apparent in WT-Tg mice (Figure 3E). Despite the increase in glycogen content, there was no difference in glycogen synthase expression between genotypes (Supplementary Figure S6). The autophagy-lysosomal pathway plays an important role in the breakdown of glycogen, as highlighted by the expansion of glycogen-filled lysosomes in lysosomal storage disorders [42]. Increased

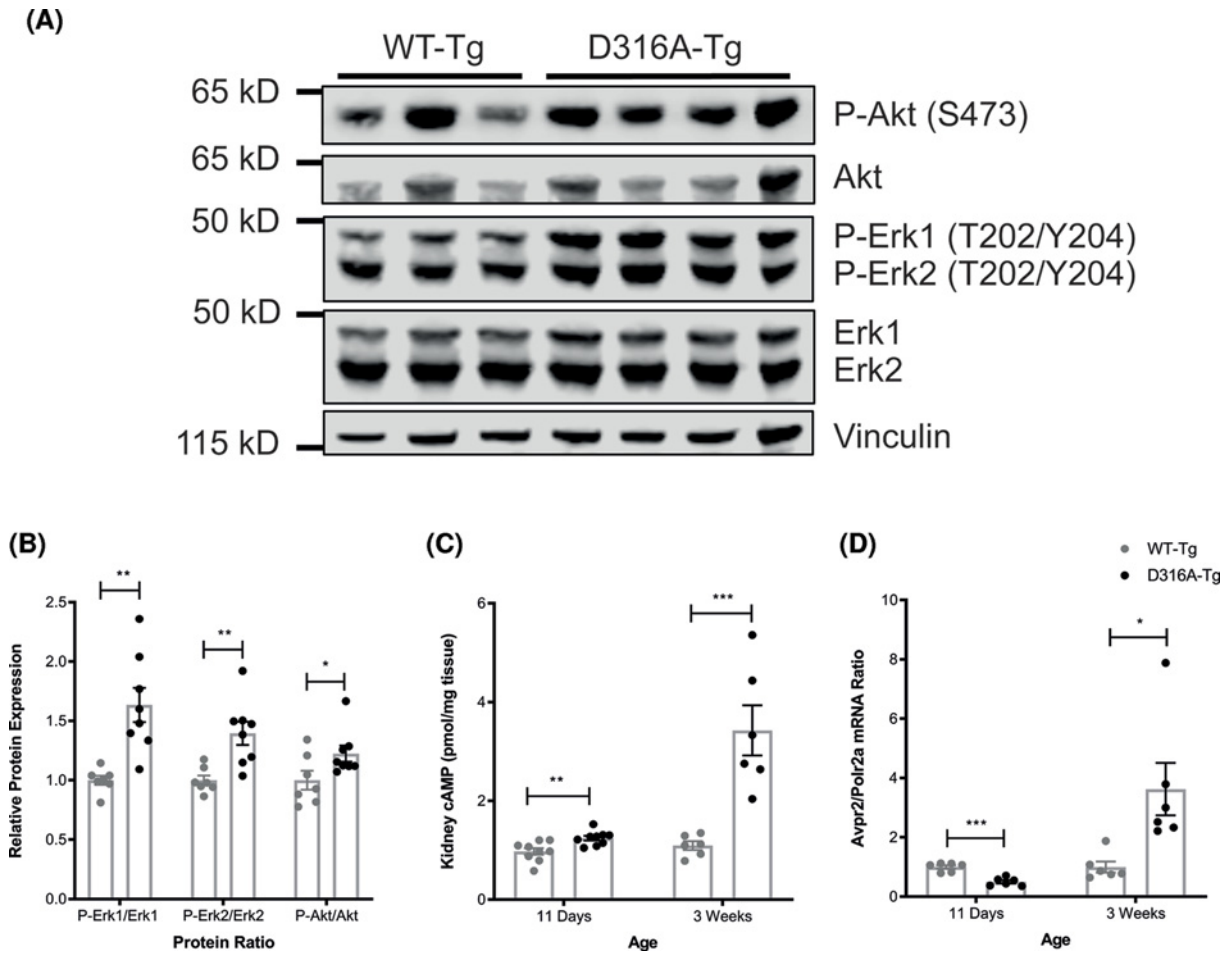

Figure 2. AMPK activation leads to increased ERK and Akt signalling and increased cAMP levels

(**A**) Phospho-Akt (S473), total Akt, phospho-Erk1/2 (T202/Y204) and total Erk1/2 levels in kidney lysates from mice aged 11 days were determined by Western blot analysis. Expression of vinculin was used as a loading control. A representative blot showing lysates isolated from three WT-Tg mice and four D316A-Tg is shown. (**B**) In each case, quantification of expression was determined and phospho-Akt and phospho-Erk1/2 levels expressed relative to total Akt/Erk1/2 levels, respectively (in each case $n \geq 7$ per genotype). Data are presented as mean ± SEM and statistically significant differences determined by Student's *t* test (*$P<0.05$, **$P<0.01$). (**C**) cAMP levels in kidneys from WT-Tg and D316A-Tg mice at 11 days and 3 weeks of age were determined ($n \geq 6$ mice per genotype and age). Data are presented as mean ± SEM and statistically significant differences between genotypes were determined by Student's *t* test (**$P<0.01$, ***$P<0.001$). (**D**) *Avpr2* gene expression in kidneys isolated from mice aged 11 days or 3 weeks ($n=6$ per genotype and age). Expression levels are plotted relative to the expression of housekeeping gene (Polr2a). Data are presented as mean ± SEM and statistical significance determined by Student's *t* test for each age group (*$P<0.05$, ***$P<0.001$).

expression of vacuolar-ATPase A (V-ATPase A), a component of the V-ATPase transporter protein known to be expressed on autophagosomes and lysosomes, was observed in kidneys from 11-day-old D316A-Tg mice compared with WT-Tg mice (Figure 3F,G). The LC3II/LC3I ratio was also decreased in D316A-Tg mice (Figure 3F,G), suggesting impaired autophagy, which has been observed in other PKD models [43,44]. Lysosomal gene expression is regulated by the MiTF/TFE family of transcription factors, of which transcription factor EB (TFEB) is a member [45,46]. Cytoplasmic–nuclear translocation of these factors enables their transcriptional activity and promotes lysosomal biogenesis [45,47]. Nuclear TFEB staining was observed in the dilating collecting ducts in D316A-Tg kidneys, whereas WT-Tg kidney sections showed cytoplasmic TFEB staining (Figure 3H). These data suggest differences in lysosomal function could be a mechanistic feature of the PKD phenotype in this model. There was no evidence for increased apoptosis, as determined by expression of cleaved caspase 3 in the kidney sections (Supplementary Figure S6).

Clinical Science (2021) **135** 2393–2408
https://doi.org/10.1042/CS20210821

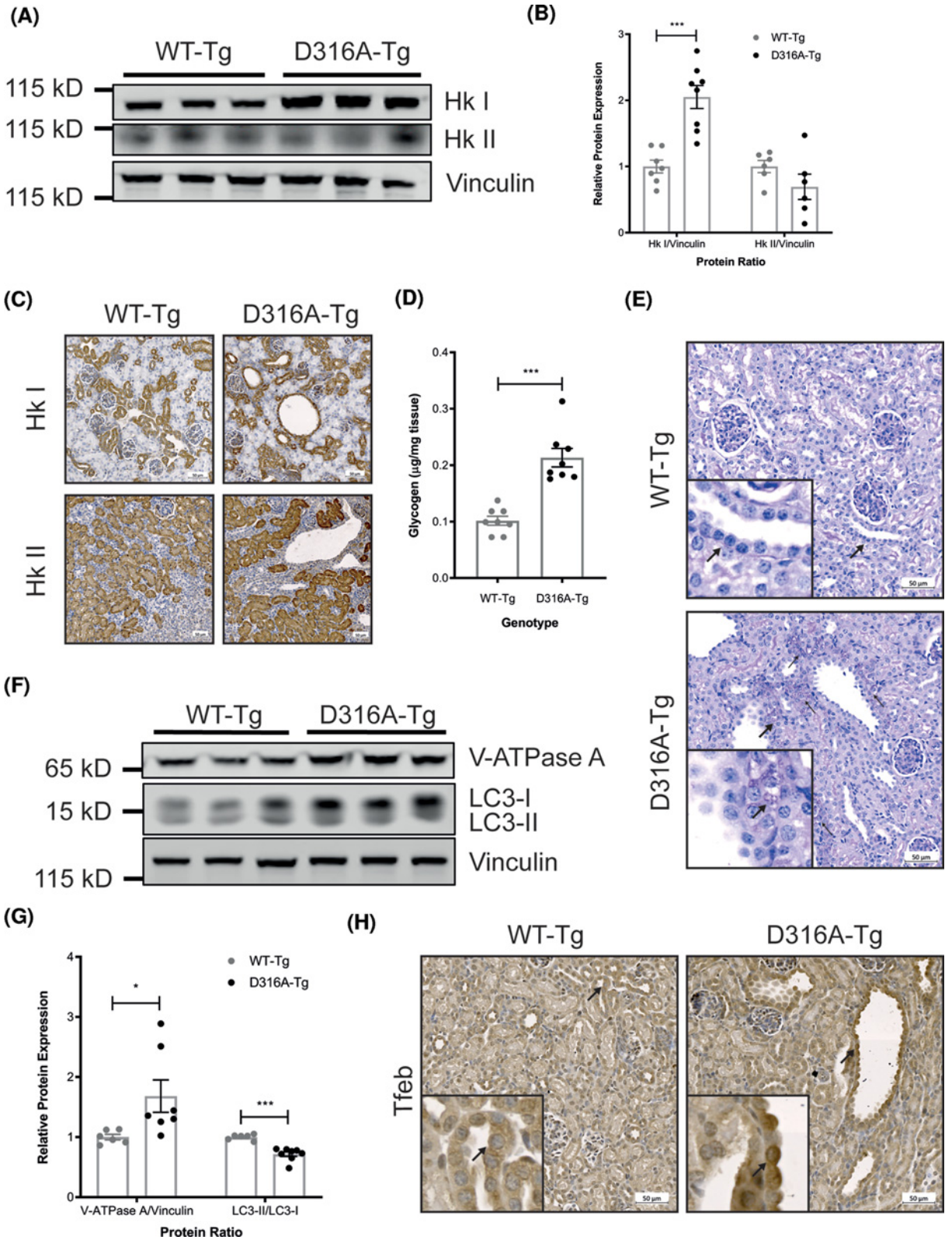

Figure 3. AMPK activation leads to increased Hk I expression and glycogen accumulation in kidney

(**A**) Kidney lysates from mice aged 11 days were probed with antibodies against Hk I, Hk II and vinculin (used as a loading control). A representative blot showing lysates isolated from three mice per genotype is shown. (**B**) In each case, expression is plotted relative to vinculin expression ($n \geq 6$ mice per genotype). Statistical significance between genotype was determined by Student's *t* test (***$P < 0.001$). (**C**) Immunohistochemical staining of kidney sections from mice aged 11 days. Sections were stained with

antibodies against Hk I (upper panel) and Hk II (lower panel). (**D**) Glycogen content of kidneys harvested from mice aged 2 weeks expressed as micrograms of glycogen per milligram of tissue (n=8 mice per genotype). Statistical significance was determined by Student's t test (***$P<0.001$). (**E**) PAS-stained kidney sections from mice aged 11 days showing glycogen accumulation (magenta). Black arrows indicate glycogen staining near cysts forming in kidneys from D316A-Tg mice that are not detected in kidneys from WT-Tg mice. Insert shows magnified regions of interest indicated by the thick blocked black arrows. (**F**) Kidney lysates from mice aged 11 days were probed with antibodies against vacuolar ATPase A (V-ATPase A), LC3 and vinculin (used as a loading control). A representative blot showing lysates isolated from three mice per genotype is shown. (**G**) Protein expression is plotted relative to vinculin expression ($n\geq6$ mice per genotype and age group). Data are presented as mean ± SEM and statistical significance determined by Student's t test for each age group (*$P<0.05$, ***$P<0.001$). (**H**) Immunohistochemical staining of kidney sections with antibodies against TFEB from mice at 11 days of age. Black arrows mark regions that are shown magnified in the inset and reveal increased nuclear staining in sections from D316A-Tg mice. For the histological data, in each case a representative image is shown for each genotype. Similar data were obtained using sections isolated from at least three other mice. Abbreviation: TFEB, transcription factor EB.

Kidney tubule-specific AMPK activation causes the polycystic kidney phenotype

Studying the global AMPK activation model raises the possibility that the PKD phenotype could arise because of AMPK activation in cell types outside the kidney. To examine this possibility, we crossed mice carrying the D316A transgene (or the WT transgene) with Ksp-Cre mice generating D316A-Tg^{Ksp} mice (and WT-Tg^{Ksp} controls). Kidneys isolated from D316A-Tg^{Ksp} mice were significantly heavier than those from WT-Tg^{Ksp} mice and cysts were clearly evident, with a significant increase in cystic index (Figure 4). These findings strongly suggest that the PKD phenotype occurs due to AMPK activation within renal tubules. Similar to the global AMPK activation model, plasma creatinine and BUN levels were significantly raised in the kidney-specific D316A-Tg^{Ksp} mice (Supplementary Figure S7). Subsequent analysis showed increased Hk I expression in D316A-Tg^{Ksp} mice compared with WT-Tg^{Ksp} control mice (Figure 4D,E), consistent with observations in the global AMPK activation model. Furthermore, glycogen content was significantly elevated in kidneys from D316A-Tg^{Ksp} mice aged 3 weeks and glycogen accumulation was observed in cells lining, or near, the cysts (Figure 4F,G). However, in contrast with the global model, there was no significant increase in cAMP levels in kidney lysates isolated from D316A-Tg^{Ksp} mice aged 3 weeks (Supplementary Figure S7), suggesting that changes in cAMP are not essential for the cystic phenotype driven by kidney-specific AMPK activation.

Expression of AMPK, Hk I and TFEB in human kidneys from ADPKD patients

The kidney phenotype observed in the AMPK gain-of-function mouse model shares similarities with that seen in ADPKD patients. We investigated the localisation of AMPK expression in the human kidney by staining for AMPKβ1, which is the most highly expressed β isoform in the kidney [15]. Figure 5 shows that AMPKβ1 is highly expressed in the collecting ducts (co-stained with Aqp2, as previously reported) [48]. Interestingly we found that, similar to the mouse, Hk I was also predominantly expressed in collecting ducts in human kidneys (Figure 5 and Supplementary Figure S8). Moreover, nuclear TFEB staining was observed in collecting duct-derived cysts in kidney sections from patients with ADPKD, whereas sections from an unaffected individual showed mainly cytoplasmic Tfeb staining (Figure 5), consistent with observations from the AMPK gain-of-function mouse model. These data highlight the possible relevance of altered AMPK, Hk I and TFEB activity to collecting duct cystogenesis in ADPKD. Finally, staining with PAS showed glycogen accumulation in cells lining, or near, the cysts in kidney sections from ADPKD patients (Figure 5 and Supplementary Figure S8) similar to the findings from the AMPK gain-of-function mouse model. Importantly, this finding provides further support for the potential role of AMPK in cystogenesis in human ADPKD.

Discussion

In the present study, we report that chronic AMPK activation in a mouse model leads to an early-onset PKD phenotype that shows similarity with human ADPKD. This phenotype was not anticipated, since previous reports indicate that AMPK activity is decreased in PKD models [49,50]. However, these studies investigated AMPK activity in the context of heavily cystic kidneys, rather than at the initiation of cystogenesis. Moreover, other studies have

Clinical Science (2021) **135** 2393–2408
https://doi.org/10.1042/CS20210821

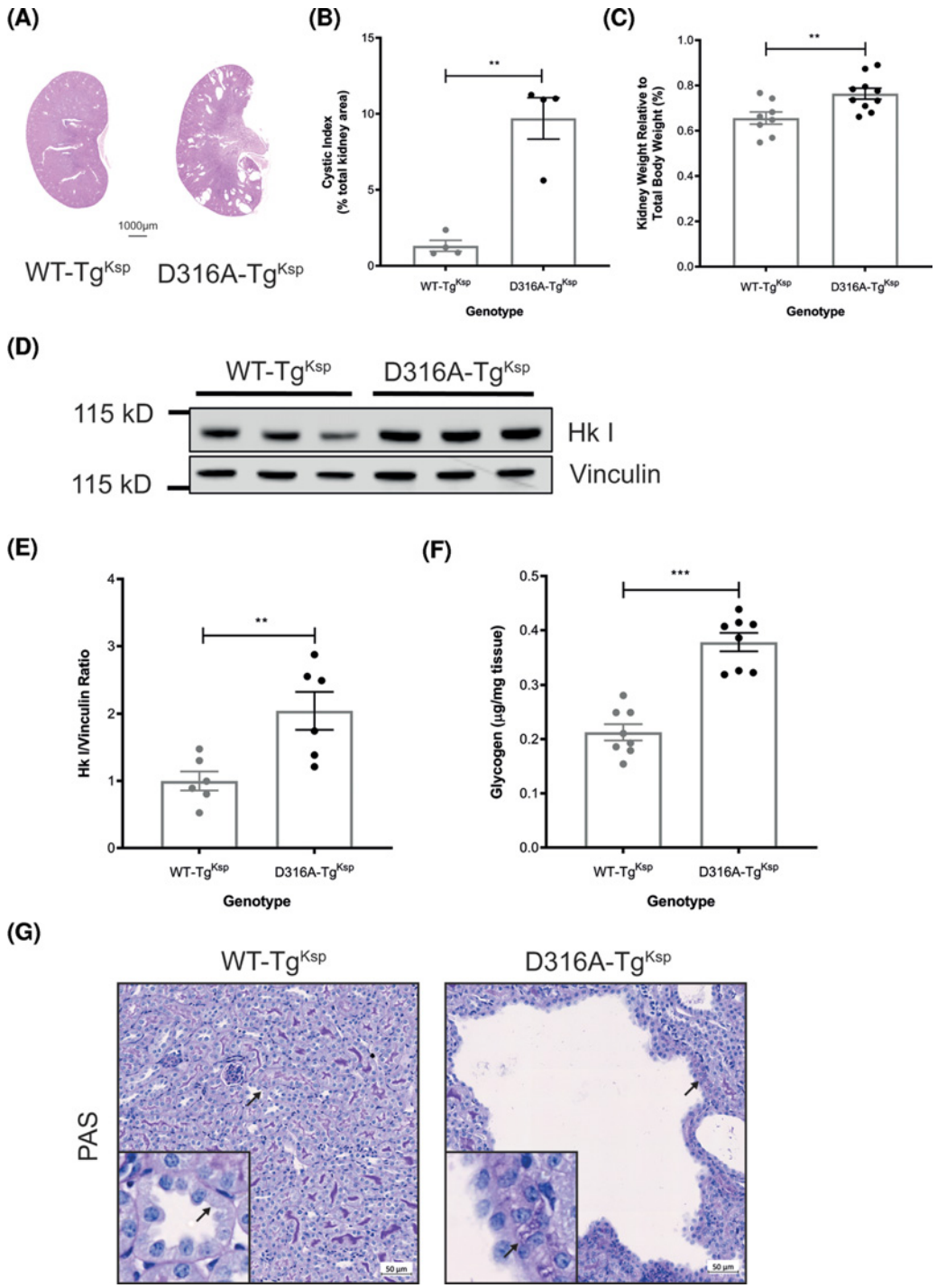

Figure 4. Kidney-specific activation of AMPK leads to a polycystic kidney phenotype

(**A**) H&E staining of kidneys harvested from D316A-Tg^{Ksp} and WT-Tg^{Ksp} mice at 3 weeks of age. A representative image of each genotype is shown. (**B**) Cystic index and (**C**) kidney weight as a percentage of total bodyweight from mice (male and female) aged 3 weeks ($n \geq 4$ per genotype). (**D**) Kidney homogenates from mice aged 11 days were probed with antibodies against Hk I and vinculin (used as a loading control) and (**E**) quantification of Hk I expression relative to vinculin ($n=6$ per genotype). (**F**) Kidney glycogen content in mice aged 3 weeks expressed as micrograms of glycogen per milligram tissue ($n=8$ mice per genotype). In all cases, data are presented as mean ± SEM and statistically significant differences between groups were determined by Student's *t* test (**$P<0.01$,***$P<0.001$). (**G**) PAS-stained kidney sections from mice aged 3 weeks with glycogen staining shown in magenta. Black arrows indicate the region magnified in the inset and show glycogen staining in cells lining, or near, cysts present in the D316A-Tg^{Ksp} mice. A representative image for each genotype is shown.

Clinical Science (2021) **135** 2393–2408
https://doi.org/10.1042/CS20210821

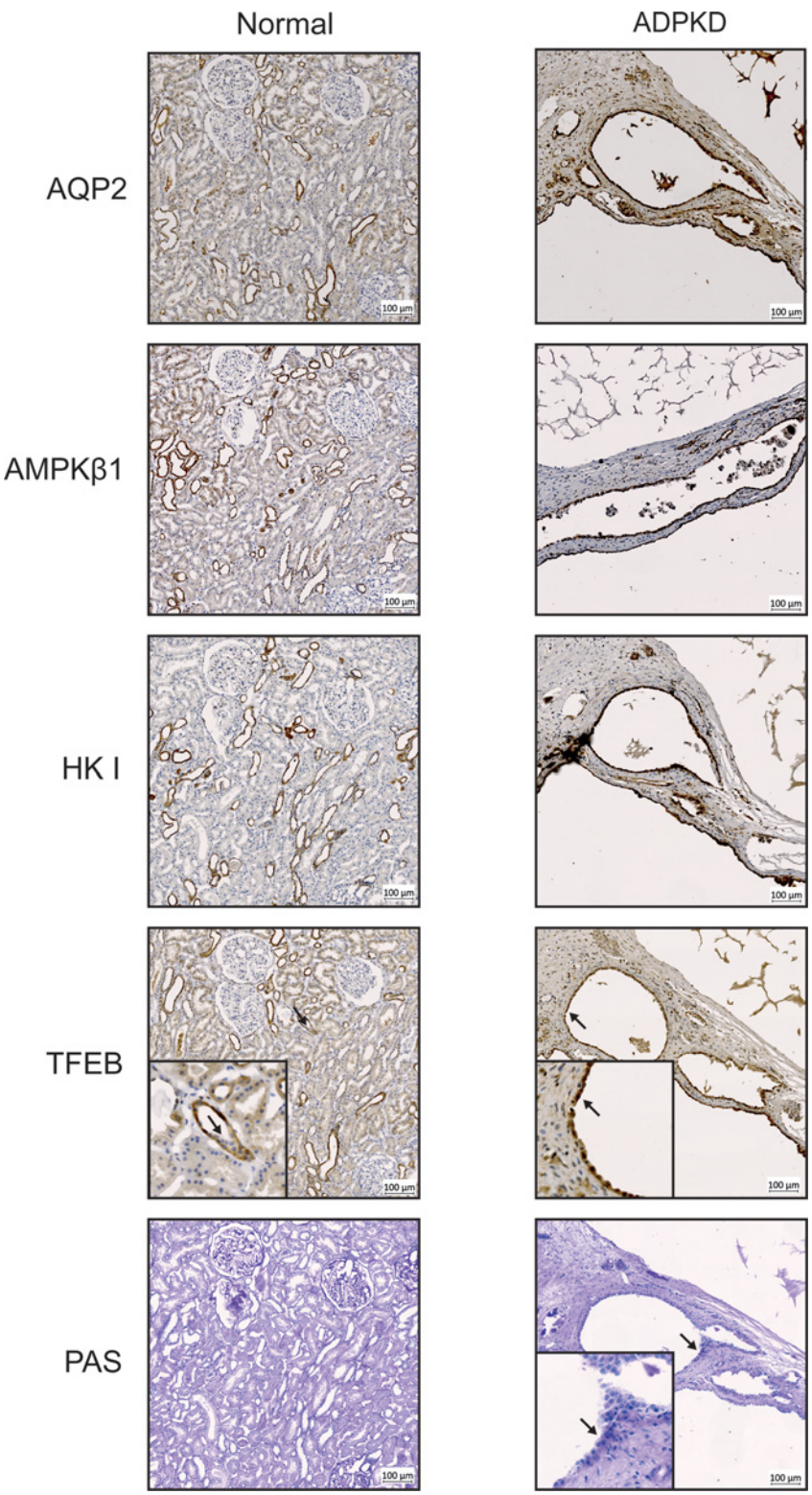

Figure 5. AMPKβ1, Hk I, TFEB and glycogen levels in human kidney sections

Images of sections from nephrectomies of a patient with late-stage ADPKD stained with antibodies against aquaporin-2 (AQP2), AMPKβ1, Hk I and TFEB or stained with PAS to reveal glycogen accumulation are shown next to corresponding images of sections from an individual without ADPKD. The black arrows in the sections stained for TFEB and PAS indicate regions that are shown magnified in the insets, and show increased nuclear staining of TFEB and glycogen accumulation in cells lining, or near, the cyst, in the ADPKD patient.

Clinical Science (2021) **135** 2393–2408
https://doi.org/10.1042/CS20210821

suggested that activation of AMPK might slow renal cystogenesis, providing a potential therapeutic approach for PKD [13,51–54]. Of note, in these studies non-specific approaches were used to activate AMPK (e.g. metformin, 2-deoxyglucose), so it is possible that AMPK-independent mechanisms could have contributed to the reported effects. For example, metformin has been shown to inhibit cAMP production in hepatocytes independently of AMPK [55]. A recent study compared the effects of metformin, canagliflozin and salsalate, together with combined metformin treatments in an adult-onset mouse model of PKD [56]. Treatment with salsalate alone resulted in the greatest degree of protection. Whilst salsalate is the prodrug of salicylate, a direct activator of AMPK, it has AMPK-independent effects and so interpreting the results of the present study is complicated. Nonetheless, it is possible that activation of AMPK following the onset of cyst development could reduce cyst progression. This could potentially offer an explanation for the reduction in cystic index that we observed in older mice (Figure 1B). How AMPK activation reduces cyst development in adult mice once cystogenesis has been initiated is unclear, but could potentially involve increased cyst drainage. Further studies investigating this mechanism could have important clinical implications for slowing PKD progression.

A previous study described a kidney phenotype featuring cyst formation and impaired renal function in a mouse model expressing an activating mutation (R528G) in the $\gamma 2$ subunit of AMPK [18]. Most of the cysts that were identified in our current study originated from collecting ducts, consistent with the AMPK$\gamma 2^{RG}$ model [18]. The time course of cystogenesis was not studied in the $\gamma 2^{RG}$ model, however cysts were reported in mice aged 26 weeks when fed a high-fat diet [18]. In contrast, the $\gamma 1$ model has a more dramatic phenotype, with earlier onset PKD that is present from less than 2 weeks *postpartum*. Other $\gamma 2$ knock-in models expressing activating N485I or R299Q mutations did not lead to a detectable kidney phenotype or a kidney phenotype was not reported [18,57]. The difference in the kidney phenotype in these models is unclear, however, one possibility could be related to different levels of AMPK activity in the models. The $\gamma 2^{RG}$ mutant was reported to have higher AMPK activity compared with the $\gamma 2^{NI}$ mutant [18]. Furthermore, AMPK$\gamma 1$-containing complexes contribute approximately 80% of total AMPK activity in rodent kidneys [58] so the $\gamma 2$ knock-in models would be predicted to have considerably less AMPK activity compared with the $\gamma 1$ model. These observations imply that a threshold level of AMPK activation is required to initiate renal cystogenesis. Moreover, the $\gamma 2^{RG}$ mutant had increased kidney glycogen accumulation similar to our model, whereas the $\gamma 2^{NI}$ mutant did not [18]. This is consistent with the hypothesis that glycogen accumulation may be a contributing factor in cystogenesis, supported by previous observations that renal glycogen accumulation is sufficient to induce cystogenesis [59,60]. Our preliminary data showing glycogen accumulation in kidney sections from patients with ADPKD suggests that the AMPK activation mouse may be a useful model for understanding the progression of ADPKD, particularly the potential for changes in metabolic pathways contributing to the disease.

There was no evidence for changes in the expression of *Pkd1*, *Pkd2* or *Pkhd1*, the primary genetic defects in PKD in humans. However, the possibility of AMPK activation affecting post-translational modification of the protein products of these genes was not studied, so this cannot be ruled out as a potential mechanism. Increased Akt and Erk signalling have previously been implicated in PKD pathogenesis [61–64] and both of these pathways were activated by 11 days of age in the D316A-Tg mice, when tubule dilations were evident. Increased cAMP levels were also detected in kidneys from the global D316A-Tg model, which was strikingly evident by 3 weeks of age, consistent with the notion that cAMP levels rise in parallel with PKD severity [65]. However, there was no significant change in cAMP levels in the kidney-specific AMPK model, suggesting that changes in cAMP signalling are not essential for AMPK-mediated cystogenesis.

Following AMPK activation, we observed increased renal expression of Hk I but not Hk II. This is consistent with a previous study showing that Hk I, but not Hk II, gene expression is up-regulated in PKD tissues [50]. Interestingly, immunohistochemical studies revealed that Hk I was expressed predominantly in the distal nephron of the mouse kidney, whereas Hk II expression was most prominent in the proximal tubules. The renal expression pattern of Hk has been incompletely delineated [66], however this proximal tubular pattern of Hk II staining has been reported previously [67]. We noted a similar pattern of HK I staining in human kidney sections. AMPK activation has been shown to lead to increased glucose uptake [68] which would be consistent with an increase in Hk expression. Cystic kidneys have also been reported to have an increased dependence on glycolysis, as inhibiting glucose metabolism alleviates PKD progression [49,50,54,69]. Localisation of Hk I expression to the cyst-forming tubules in the D316A-Tg model and the known glycolytic dependence of PKD could indicate that increased Hk I expression may contribute to the mechanism of cystogenesis.

Altered expression of autophagic proteins and nuclear expression of TFEB in the dilating tubules was noted in D316A-Tg kidneys. Nuclear TFEB staining was also observed in collecting duct cysts in human ADPKD kidney sections. To our knowledge, this is the first report indicating increased nuclear TFEB expression in ADPKD cyst-lining

cells. Previous studies have reported that activation of AMPK increases nuclear translocation of TFEB [70–73]. Increased nuclear Tfe3 expression has been observed in a folliculin (*Flcn*) knockout mouse model, which presents with a PKD phenotype [74–76]. Furthermore, a PKD phenotype featuring collecting duct cysts was reported in a kidney-specific TFEB overexpression model, suggesting that dysregulated TFEB/Tfe3 signalling is sufficient to drive renal cystogenesis [77]. Very recently, constitutive activation of TFEB was reported to be a key driver of kidney abnormalities in a mouse model of Birt–Hogg–Dube syndrome [78] including increased kidney cystogenesis. In the future it will be interesting to investigate whether AMPK-mediated regulation of the TFEB/Tfe3 pathway has a mechanistic role in PKD pathogenesis.

There is growing interest in the role of metabolism in PKD pathogenesis, and the potential it brings for identifying therapeutic targets [79]. Previous reports have highlighted the possibility of activating AMPK pharmacologically to treat PKD. This idea was predicated on reports of lower levels of AMPK activity in cystic kidneys coupled with the antagonistic effect of AMPK on mTOR signalling, a major driver of cyst progression [4,5,49,79]. Consequently, the metabolic changes that occur in PKD have been suggested to be due primarily to up-regulated mTOR signaling [50,80]. In this study, we show that chronic AMPK activation *per se* causes a PKD phenotype in mice. It will be important to determine whether established genetic mutations that cause PKD result in AMPK activation and whether this is required for the metabolic reprogramming seen in PKD to drive cystogenesis.

Clinical perspectives

- The role of AMPK in regulating kidney function is incompletely understood and in the present study we used a genetic gain-of-function AMPK mouse model to investigate the effect of chronic AMPK activation in the kidney.
- Our findings reveal that chronic activation of AMPK leads to an early-onset PKD, with striking similarity to human ADPKD.
- These findings have significant implications not only for future studies aimed at mechanistic understanding of human kidney disease, but also for potential therapeutic intervention.

Data Availability

All supporting data are included within the main manuscript and its supplementary files.

Competing Interests

The authors declare that there are no competing interests associated with the manuscript.

Funding

This work was supported by a Ph.D. Studentship from the British Heart Foundation as part of a Centre of Excellence Award to Imperial College [grant number FS/14/62/31288 (to Laura Wilson)]; and the Medical Research Council U.K. [grant number MC-A654-5QB10].

Open Access

Open access for this article was enabled by the participation of Imperial College London in an all-inclusive *Read & Publish* pilot with Portland Press and the Biochemical Society under a transformative agreement with JISC.

CRediT Author Contribution

Laura Wilson: Conceptualisation, Data curation, Investigation, Methodology, Writing—original draft, Writing—review & editing. **Alice E. Pollard:** Investigation, Methodology, Writing—original draft, Writing—review & editing. **Lucy Penfold:** Investigation, Writing—original draft, Writing—review & editing. **Phillip J. Muckett:** Investigation, Writing—review & editing. **Chad Whilding:** Software, Investigation, Writing—review & editing. **Mohammad Bohlooly-Y.:** Conceptualisation, Investigation, Writing—review & editing. **Patricia Wilson:** Resources, Methodology, Writing—review & editing. **David Carling:** Conceptualisation, Resources, Formal analysis, Supervision, Funding acquisition, Methodology, Writing—original draft, Project administration, Writing—review & editing.

Clinical Science (2021) **135** 2393–2408
https://doi.org/10.1042/CS20210821

Acknowledgements

We are extremely grateful to Dr. Eleni Vloumidi (MRC London Institute of Medical Sciences Institute Whole Animal Physiology and Imaging Facility) for expert assistance with the blood pressure measurements. We are indebted to the PKD Charity, U.K. for their donation of samples from their PKD Bioresource Bank.

Abbreviations

ACC, acetyl-CoA carboxylase; ADPKD, autosomal dominant polycystic kidney disease; AMPK, AMP-activated protein kinase; BUN, blood urea nitrogen; CFTR, cystic fibrosis transmembrane conductance regulator; eGFR, estimated glomerular filtration rate; Hk I, hexokinase I; Hk II, hexokinase II; H&E, Haematoxylin and Eosin; Kim 1, kidney injury molecule 1; mTOR, mammalian target of rapamycin; Ngal, neutrophil gelatinase-associated lipocalin; PAS, Periodic Acid–Schiff; Pgc1α, peroxisome proliferator activated receptor-γ co-activator 1α; PKD, polycystic kidney disease; TFEB, transcription factor EB.

References

1 Steinberg, G.R. and Carling, D. (2019) AMP-activated protein kinase: the current landscape for drug development. *Nat. Rev. Drug Discov.* **18**, 527–551, https://doi.org/10.1038/s41573-019-0019-2
2 Carling, D. (2017) AMPK signalling in health and disease. *Curr. Opin. Cell Biol.* **45**, 31–37, https://doi.org/10.1016/j.ceb.2017.01.005
3 Jager, S. et al. (2007) AMP-activated protein kinase (AMPK) action in skeletal muscle via direct phosphorylation of PGC-1alpha. *Proc. Natl. Acad. Sci. U.S.A.* **104**, 12017–12022, https://doi.org/10.1073/pnas.0705070104
4 Inoki, K., Zhu, T. and Guan, K.L. (2003) TSC2 mediates cellular energy response to control cell growth and survival. *Cell* **115**, 577–590, https://doi.org/10.1016/S0092-8674(03)00929-2
5 Gwinn, D.M. et al. (2008) AMPK phosphorylation of raptor mediates a metabolic checkpoint. *Mol. Cell* **30**, 214–226, https://doi.org/10.1016/j.molcel.2008.03.003
6 Hunter, R.W. et al. (2011) Molecular mechanism by which AMP-activated protein kinase activation promotes glycogen accumulation in muscle. *Diabetes* **60**, 766–774, https://doi.org/10.2337/db10-1148
7 Hallows, K.R. et al. (2000) Inhibition of cystic fibrosis transmembrane conductance regulator by novel interaction with the metabolic sensor AMP-activated protein kinase. *J. Clin. Invest.* **105**, 1711–1721, https://doi.org/10.1172/JCI9622
8 King, Jr, J.D. et al. (2009) AMP-activated protein kinase phosphorylation of the R domain inhibits PKA stimulation of CFTR. *Am. J. Physiol. Cell Physiol.* **297**, C94–C101, https://doi.org/10.1152/ajpcell.00677.2008
9 Kongsuphol, P. et al. (2009) Regulation of Cl(-) secretion by AMPK in vivo. *Pflugers Arch.* **457**, 1071–1078, https://doi.org/10.1007/s00424-008-0577-3
10 Almaca, J. et al. (2009) AMPK controls epithelial Na(+) channels through Nedd4-2 and causes an epithelial phenotype when mutated. *Pflugers Arch.* **458**, 713–721, https://doi.org/10.1007/s00424-009-0660-4
11 Bhalla, V. et al. (2006) AMP-activated kinase inhibits the epithelial Na+ channel through functional regulation of the ubiquitin ligase Nedd4-2. *J. Biol. Chem.* **281**, 26159–26169, https://doi.org/10.1074/jbc.M606045200
12 Carattino, M.D. et al. (2005) Epithelial sodium channel inhibition by AMP-activated protein kinase in oocytes and polarized renal epithelial cells. *J. Biol. Chem.* **280**, 17608–17616, https://doi.org/10.1074/jbc.M501770200
13 Takiar, V. et al. (2011) Activating AMP-activated protein kinase (AMPK) slows renal cystogenesis. *Proc. Natl. Acad. Sci. U.S.A.* **108**, 2462–2467, https://doi.org/10.1073/pnas.1011498108
14 Lee, M. et al. (2018) Phosphorylation of acetyl-CoA carboxylase by AMPK reduces renal fibrosis and is essential for the anti-fibrotic effect of metformin. *J. Am. Soc. Nephrol.* **29**, 2326–2336, https://doi.org/10.1681/ASN.2018010050
15 Salatto, C.T. et al. (2017) Selective Activation of AMPK beta1-containing isoforms improves kidney function in a rat model of diabetic nephropathy. *J. Pharmacol. Exp. Ther.* **361**, 303–311, https://doi.org/10.1124/jpet.116.237925
16 Zhou, X. et al. (2019) PAN-AMPK activation improves renal function in a rat model of progressive diabetic nephropathy. *J. Pharmacol. Exp. Ther.* **371**, 45–55, https://doi.org/10.1124/jpet.119.258244
17 Fang, Y. et al. (2020) Metformin effectively treats Tsc1 deletion-caused kidney pathology by upregulating AMPK phosphorylation. *Cell Death Discov.* **6**, 52, https://doi.org/10.1038/s41420-020-0285-0
18 Yang, X. et al. (2016) Physiological expression of AMPKgamma2RG mutation causes Wolff-Parkinson-White syndrome and induces kidney injury in mice. *J. Biol. Chem.* **291**, 23428–23439, https://doi.org/10.1074/jbc.M116.738591
19 Woods, A. et al. (2017) Liver-specific activation of AMPK prevents steatosis on a high-fructose diet. *Cell Rep.* **18**, 3043–3051, https://doi.org/10.1016/j.celrep.2017.03.011
20 Shao, X. et al. (2002) A minimal Ksp-cadherin promoter linked to a green fluorescent protein reporter gene exhibits tissue-specific expression in the developing kidney and genitourinary tract. *J. Am. Soc. Nephrol.* **13**, 1824–1836, https://doi.org/10.1097/01.ASN.0000016443.50138.CD
21 Shao, X., Somlo, S. and Igarashi, P. (2002) Epithelial-specific Cre/lox recombination in the developing kidney and genitourinary tract. *J. Am. Soc. Nephrol.* **13**, 1837–1846, https://doi.org/10.1097/01.ASN.0000016444.90348.50
22 Pollard, A.E. et al. (2019) AMPK activation protects against diet induced obesity through Ucp1-independent thermogenesis in subcutaneous white adipose tissue. *Nat. Metab.* **1**, 340–349, https://doi.org/10.1038/s42255-019-0036-9
23 Reeders, S.T. et al. (1985) A highly polymorphic DNA marker linked to adult polycystic kidney disease on chromosome 16. *Nature* **317**, 542–544, https://doi.org/10.1038/317542a0

24 Hughes, J. et al. (1995) The polycystic kidney disease 1 (PKD1) gene encodes a novel protein with multiple cell recognition domains. *Nat. Genet.* **10**, 151–160, https://doi.org/10.1038/ng0695-151
25 Mochizuki, T. et al. (1996) PKD2, a gene for polycystic kidney disease that encodes an integral membrane protein. *Science* **272**, 1339–1342, https://doi.org/10.1126/science.272.5266.1339
26 Ward, C.J. et al. (2002) The gene mutated in autosomal recessive polycystic kidney disease encodes a large, receptor-like protein. *Nat. Genet.* **30**, 259–269, https://doi.org/10.1038/ng833
27 Nagasawa, Y. et al. (2002) Identification and characterization of Pkhd1, the mouse orthologue of the human ARPKD gene. *J. Am. Soc. Nephrol.* **13**, 2246–2258, https://doi.org/10.1097/01.ASN.0000030392.19694.9D
28 Yamaguchi, T. et al. (2003) Cyclic AMP activates B-Raf and ERK in cyst epithelial cells from autosomal-dominant polycystic kidneys. *Kidney Int.* **63**, 1983–1994, https://doi.org/10.1046/j.1523-1755.2003.00023.x
29 Yamaguchi, T. et al. (2004) Calcium restriction allows cAMP activation of the B-Raf/ERK pathway, switching cells to a cAMP-dependent growth-stimulated phenotype. *J. Biol. Chem.* **279**, 40419–40430, https://doi.org/10.1074/jbc.M405079200
30 Belibi, F.A. et al. (2004) Cyclic AMP promotes growth and secretion in human polycystic kidney epithelial cells. *Kidney Int.* **66**, 964–973, https://doi.org/10.1111/j.1523-1755.2004.00843.x
31 Smith, L.A. et al. (2006) Development of polycystic kidney disease in juvenile cystic kidney mice: insights into pathogenesis, ciliary abnormalities, and common features with human disease. *J. Am. Soc. Nephrol.* **17**, 2821–2831, https://doi.org/10.1681/ASN.2006020136
32 Starremans, P.G. et al. (2008) A mouse model for polycystic kidney disease through a somatic in-frame deletion in the 5' end of Pkd1. *Kidney Int.* **73**, 1394–1405, https://doi.org/10.1038/ki.2008.111
33 Gattone, II, V.H. et al. (2003) Inhibition of renal cystic disease development and progression by a vasopressin V2 receptor antagonist. *Nat. Med.* **9**, 1323–1326, https://doi.org/10.1038/nm935
34 Torres, V.E. et al. (2004) Effective treatment of an orthologous model of autosomal dominant polycystic kidney disease. *Nat. Med.* **10**, 363–364, https://doi.org/10.1038/nm1004
35 Wallace, D.P. (2011) Cyclic AMP-mediated cyst expansion. *Biochim. Biophys. Acta* **1812**, 1291–1300, https://doi.org/10.1016/j.bbadis.2010.11.005
36 Wang, X. et al. (2005) Effectiveness of vasopressin V2 receptor antagonists OPC-31260 and OPC-41061 on polycystic kidney disease development in the PCK rat. *J. Am. Soc. Nephrol.* **16**, 846–851, https://doi.org/10.1681/ASN.2004121090
37 Wu, Z. et al. (1999) Mechanisms controlling mitochondrial biogenesis and respiration through the thermogenic coactivator PGC-1. *Cell* **98**, 115–124, https://doi.org/10.1016/S0092-8674(00)80611-X
38 Menezes, L.F. and Germino, G.G. (2019) The pathobiology of polycystic kidney disease from a metabolic viewpoint. *Nat. Rev. Nephrol.* **15**, 735–749, https://doi.org/10.1038/s41581-019-0183-y
39 Menezes, L.F. et al. (2016) Fatty acid oxidation is impaired in an orthologous mouse model of autosomal dominant polycystic kidney disease. *EBioMedicine* **5**, 183–192, https://doi.org/10.1016/j.ebiom.2016.01.027
40 Hajarnis, S. et al. (2017) microRNA-17 family promotes polycystic kidney disease progression through modulation of mitochondrial metabolism. *Nat. Commun.* **8**, 14395, https://doi.org/10.1038/ncomms14395
41 Ishimoto, Y. et al. (2017) Mitochondrial abnormality facilitates cyst formation in autosomal dominant polycystic kidney disease. *Mol. Cell. Biol.* **37**, e00337–17, https://doi.org/10.1128/MCB.00337-17
42 Lim, J.A., Li, L. and Raben, N. (2014) Pompe disease: from pathophysiology to therapy and back again. *Front. Aging Neurosci.* **6**, 177, https://doi.org/10.3389/fnagi.2014.00177
43 Ravichandran, K. and Edelstein, C.L. (2014) Polycystic kidney disease: a case of suppressed autophagy? *Semin. Nephrol.* **34**, 27–33, https://doi.org/10.1016/j.semnephrol.2013.11.005
44 Zhu, P. et al. (2017) Autophagy activators suppress cystogenesis in an autosomal dominant polycystic kidney disease model. *Hum. Mol. Genet.* **26**, 158–172
45 Sardiello, M. et al. (2009) A gene network regulating lysosomal biogenesis and function. *Science* **325**, 473–477, https://doi.org/10.1126/science.1174447
46 Settembre, C. et al. (2011) TFEB links autophagy to lysosomal biogenesis. *Science* **332**, 1429–1433, https://doi.org/10.1126/science.1204592
47 Martina, J.A. et al. (2014) The nutrient-responsive transcription factor TFE3 promotes autophagy, lysosomal biogenesis, and clearance of cellular debris. *Sci. Signal.* **7**, ra9, https://doi.org/10.1126/scisignal.2004754
48 Devuyst, O. et al. (1996) Expression of aquaporins-1 and -2 during nephrogenesis and in autosomal dominant polycystic kidney disease. *Am. J. Physiol.* **271**, F169–F183, https://doi.org/10.1152/ajprenal.1996.271.1.F169
49 Riwanto, M. et al. (2016) Inhibition of aerobic glycolysis attenuates disease progression in polycystic kidney disease. *PLoS ONE* **11**, e0146654, https://doi.org/10.1371/journal.pone.0146654
50 Rowe, I. et al. (2013) Defective glucose metabolism in polycystic kidney disease identifies a new therapeutic strategy. *Nat. Med.* **19**, 488–493, https://doi.org/10.1038/nm.3092
51 Chang, M.Y. et al. (2017) Metformin inhibits cyst formation in a zebrafish model of polycystin-2 deficiency. *Sci. Rep.* **7**, 7161, https://doi.org/10.1038/s41598-017-07300-x
52 Seliger, S.L. et al. (2018) A randomized clinical trial of metformin to treat autosomal dominant polycystic kidney disease. *Am. J. Nephrol.* **47**, 352–360, https://doi.org/10.1159/000488807
53 Warner, G. et al. (2016) Food restriction ameliorates the development of polycystic kidney disease. *J. Am. Soc. Nephrol.* **27**, 1437–1447, https://doi.org/10.1681/ASN.2015020132
54 Zhao, J. et al. (2019) Low-dose 2-deoxyglucose and metformin synergically inhibit proliferation of human polycystic kidney cells by modulating glucose metabolism. *Cell Death Discov.* **5**, 76, https://doi.org/10.1038/s41420-019-0156-8

Clinical Science (2021) **135** 2393–2408
https://doi.org/10.1042/CS20210821

55 Miller, R.A. et al. (2013) Biguanides suppress hepatic glucagon signalling by decreasing production of cyclic AMP. *Nature* **494**, 256–260, https://doi.org/10.1038/nature11808
56 Leonhard, W.N. et al. (2019) Salsalate, but not metformin or canagliflozin, slows kidney cyst growth in an adult-onset mouse model of polycystic kidney disease. *EBioMedicine* **47**, 436–445, https://doi.org/10.1016/j.ebiom.2019.08.041
57 Yavari, A. et al. (2016) Chronic activation of gamma2 AMPK induces obesity and reduces beta cell function. *Cell Metab.* **23**, 821–836, https://doi.org/10.1016/j.cmet.2016.04.003
58 Cheung, P.C. et al. (2000) Characterization of AMP-activated protein kinase gamma-subunit isoforms and their role in AMP binding. *Biochem. J.* **346 Pt 3**, 659–669, https://doi.org/10.1042/bj3460659
59 Gjorgjieva, M. et al. (2016) Progressive development of renal cysts in glycogen storage disease type I. *Hum. Mol. Genet.* **25**, 3784–3797, https://doi.org/10.1093/hmg/ddw224
60 Gjorgjieva, M. et al. (2018) Polycystic kidney features of the renal pathology in glycogen storage disease type I: possible evolution to renal neoplasia. *J. Inherit. Metab. Dis.* **41**, 955–963, https://doi.org/10.1007/s10545-018-0207-y
61 Nagao, S. et al. (2003) Renal activation of extracellular signal-regulated kinase in rats with autosomal-dominant polycystic kidney disease. *Kidney Int.* **63**, 427–437, https://doi.org/10.1046/j.1523-1755.2003.00755.x
62 Nishio, S. et al. (2005) Pkd1 regulates immortalized proliferation of renal tubular epithelial cells through p53 induction and JNK activation. *J. Clin. Invest.* **115**, 910–918, https://doi.org/10.1172/JCI22850
63 Shibazaki, S. et al. (2008) Cyst formation and activation of the extracellular regulated kinase pathway after kidney specific inactivation of Pkd1. *Hum. Mol. Genet.* **17**, 1505–1516, https://doi.org/10.1093/hmg/ddn039
64 Wahl, P.R. et al. (2007) Mitotic activation of Akt signalling pathway in Han:SPRD rats with polycystic kidney disease. *Nephrology (Carlton)* **12**, 357–363, https://doi.org/10.1111/j.1440-1797.2007.00811.x
65 Smith, L.A. et al. (2006) Development of polycystic kidney disease in juvenile cystic kidney mice: insights into pathogenesis, ciliary abnormalities, and common features with human disease. *J. Am. Soc. Nephrol.* **17**, 2821–2831, https://doi.org/10.1681/ASN.2006020136
66 Robey, R.B. (2011) Hexokinase: a novel sugar kinase coupled to renal epithelial cell survival. *Kidney Int.* **79**, 1163–1165, https://doi.org/10.1038/ki.2011.20
67 Gall, J.M. et al. (2011) Hexokinase regulates Bax-mediated mitochondrial membrane injury following ischemic stress. *Kidney Int.* **79**, 1207–1216, https://doi.org/10.1038/ki.2010.532
68 Cokorinos, E.C. et al. (2017) Activation of skeletal muscle AMPK promotes glucose disposal and glucose lowering in non-human primates and mice. *Cell Metab.* **25**, 1147.e10–1159.e10, https://doi.org/10.1016/j.cmet.2017.04.010
69 Chiaravalli, M. et al. (2016) 2-Deoxy-d-glucose ameliorates PKD progression. *J. Am. Soc. Nephrol.* **27**, 1958–1969, https://doi.org/10.1681/ASN.2015030231
70 Roczniak-Ferguson, A. et al. (2012) The transcription factor TFEB links mTORC1 signaling to transcriptional control of lysosome homeostasis. *Sci. Signal.* **5**, ra42, https://doi.org/10.1126/scisignal.2002790
71 Young, N.P. et al. (2016) AMPK governs lineage specification through Tfeb-dependent regulation of lysosomes. *Genes Dev.* **30**, 535–552, https://doi.org/10.1101/gad.274142.115
72 El-Houjeiri, L. et al. (2019) The transcription factors TFEB and TFE3 link the FLCN-AMPK signaling axis to innate immune response and pathogen resistance. *Cell Rep.* **26**, 3613.e6–3628.e6, https://doi.org/10.1016/j.celrep.2019.02.102
73 Collodet, C. et al. (2019) AMPK promotes induction of the tumor suppressor FLCN through activation of TFEB independently of mTOR. *FASEB J.* **33**, 12374–12391, https://doi.org/10.1096/fj.201900841R
74 Baba, M. et al. (2008) Kidney-targeted Birt-Hogg-Dube gene inactivation in a mouse model: Erk1/2 and Akt-mTOR activation, cell hyperproliferation, and polycystic kidneys. *J. Natl. Cancer Inst.* **100**, 140–154, https://doi.org/10.1093/jnci/djm288
75 Chen, J. et al. (2008) Deficiency of FLCN in mouse kidney led to development of polycystic kidneys and renal neoplasia. *PLoS ONE* **3**, e3581, https://doi.org/10.1371/journal.pone.0003581
76 Hong, S.B. et al. (2010) Inactivation of the FLCN tumor suppressor gene induces TFE3 transcriptional activity by increasing its nuclear localization. *PLoS ONE* **5**, e15793, https://doi.org/10.1371/journal.pone.0015793
77 Calcagni, A. et al. (2016) Modelling TFE renal cell carcinoma in mice reveals a critical role of WNT signaling. *eLife* **5**, e17047, https://doi.org/10.7554/eLife.17047
78 Napolitano, G. et al. (2020) A substrate-specific mTORC1 pathway underlies Birt-Hogg-Dube syndrome. *Nature* **585**, 597–602, https://doi.org/10.1038/s41586-020-2444-0
79 Padovano, V. et al. (2018) Metabolism and mitochondria in polycystic kidney disease research and therapy. *Nat. Rev. Nephrol.* **14**, 678–687, https://doi.org/10.1038/s41581-018-0051-1
80 Priolo, C. and Henske, E.P. (2013) Metabolic reprogramming in polycystic kidney disease. *Nat. Med.* **19**, 407–409, https://doi.org/10.1038/nm.3140